ENVIRONMENTAL RESEARCH
LETTERS

LETTER

Mechanisms of high-temperature ozone suppression in Eastern China: a meteorological perspective

Nan Li[1,2,*], **Jianping Liang**[1], **Wanwan Liu**[1], **Chengkai Gu**[3], **Jiandong Li**[1], **Yang Xu**[1], **Keqin Tang**[1], **Hong Liao**[1] **and Jianlin Hu**[1]

[1] Jiangsu Key Laboratory of Atmospheric Environment Monitoring and Pollution Control, Jiangsu Collaborative Innovation Center of Atmospheric Environment and Equipment Technology, School of Environmental Science and Engineering, Nanjing University of Information Science & Technology, Nanjing, People's Republic of China
[2] Key Laboratory of Formation and Prevention of Urban Air Pollution Complex, Ministry of Ecology and Environment, Shanghai, People's Republic of China
[3] Meteorological Bureau, Dalian Air Traffic Management Station of Civil Aviation Administration of China, Dalian, People's Republic of China
[*] Author to whom any correspondence should be addressed.

E-mail: linan@nuist.edu.cn

OPEN ACCESS

RECEIVED
4 February 2025

REVISED
30 June 2025

ACCEPTED FOR PUBLICATION
18 July 2025

PUBLISHED
30 July 2025

Keywords: ozone pollution, high temperature, ozone suppression, meteorology, Eastern China

Supplementary material for this article is available online

Abstract

Ozone (O_3) is a typical secondary photochemical pollutant, whose production typically increases under high temperature and radiation. However, emerging observational evidences reveal a notable alteration in the O_3-temperature relationship under extremely heat conditions (referred to as O_3 suppression) in 20%–30% cities of China, yet the underlying mechanisms and driving forces remain unclear. This study provides a comprehensive investigation of the meteorological mechanisms driving high-temperature O_3 suppression in Eastern China, with particular emphasis on regional disparities between suppression and non-suppression areas. Our analysis revealed distinct spatial patterns of O_3 suppression across major Chinese regions. The Yangtze River Delta (YRD) and Pearl River Delta (PRD) regions exhibit significant O_3 suppression, with the O_3-temperature relationship decreasing by 3–5 $\mu g\ m^{-3}\ ^\circ C^{-1}$ at high temperatures. In contrast, the Beijing–Tianjin–Hebei (BTH) region rarely illustrates this phenomenon. Through integrated statistical analysis and machine learning approaches, we identified radiation, relative humidity (RH), and planetary boundary layer height (PBLH) as the key meteorological drivers. Mechanistic analysis demonstrated that RH was the dominant factor accounting for regional differences in O_3 suppression, primarily owing to the contrasting effects of dry heat (BTH) and wet heat (YRD and PRD). PBLH emerged as a secondary influential factor that modulates O_3 concentration through the competitive effects of diffusion and transport processes. Cluster analysis further revealed that the occurrence frequency of inhibitory meteorological conditions (high RH and low PBLH) during high-temperature days in the YRD and PRD regions (25%–35%) significantly exceeded that in the BTH region (2%). This study provides crucial insights into the regional disparities in meteorological mechanisms underlying high-temperature O_3 suppression and offers valuable scientific support for region-specific O_3 pollution control strategies in the context of climate warming and increasingly frequent heatwaves.

1. Introduction

Surface ozone (O_3) is a typical secondary gaseous pollutant produced by the photochemical oxidation of volatile organic compounds (VOCs) and nitrogen oxides (NO_x) in the presence of sunlight (Wang *et al* 2017, 2022). High O_3 concentrations significantly affect human health (Atkinson *et al* 2016, Murray *et al* 2020, Sun *et al* 2022) and agricultural production (Tai *et al* 2014, Feng *et al* 2019, 2022, Wang *et al* 2023) because of its strong oxidative properties. Over the past few decades, air pollution in China has become severe (Pu *et al* 2017, Lu *et al* 2018). Since 2017, ground-level O_3 has surpassed particulate matter as the primary pollutant affecting air quality during summer in China. Notably, megacities such as Beijing, Shanghai, Nanjing, and Guangzhou have witnessed rapid increases in O_3 concentrations, leading to severe photochemical pollution (Li *et al* 2019, Liu *et al* 2020, Mousavinezhad *et al* 2021, Xu *et al* 2021).

In general, O_3 concentration increases with increasing temperature at an approximate rate of 2–8 ppb $°C^{-1}$, which is primarily attributed to more intense solar radiation and enhanced chemical reaction at high temperatures (Gu *et al* 2020, Han *et al* 2020, Hu *et al* 2021). However, the direct correlation between O_3 and temperature may change under extremely high temperatures, resulting in a noticeable slowdown or even decrease in this trend (Ning *et al* 2022). In urban areas over central China, the O_3 concentration starts to decline at an approximate rate of $-1.5 \sim -2.0\ \mu g\ m^{-3}\ °C^{-1}$ when air temperature exceeds 32 °C (Fu *et al* 2024). Similarly, in the Yangtze River Delta (YRD) region, the O_3 concentration reaches a peak at 38 °C during the months of June to August, then gradually declines (Pu *et al* 2017). Comprehending the attributes and mechanisms of O_3 suppression is a key area of research particularly against the backdrop of global warming and increasingly frequent heatwaves (Meehl *et al* 2018, Romer *et al* 2018).

Several studies have attempted to explain the potential driving forces behind O_3 suppression at high temperatures. Steiner *et al* (2010) focused on chemical factors and hypothesized that O_3 suppression in California could be attributed to a combination of reduced NO_x sequestration by peroxyacetyl nitrate (PAN) and decreased emissions of biogenic isoprene under extremely high-temperature conditions. In a broader investigation encompassing the entire U.S., Shen *et al* (2016) showed that O_3 suppression cannot be fully explained by the hypothesis of Steiner *et al* (2010), instead predominantly arising from meteorological processes, such as solar radiation, synoptic circulation, and stagnation. In China, research has focused on the nature of O_3 suppression at high temperatures (Pu *et al* 2017, Ning *et al* 2022), with few studies investigating the mechanism and driving forces behind the phenomenon.

In this study, we explore and compare the attributes of O_3 suppression under high-temperature conditions during 2016–2020 in three typical regions of Eastern China: Beijing–Tianji–Hebei (BTH), Pearl River Delta (PRD) and YRD. We then identify the meteorological factors driving this phenomenon and compare distinct regional disparities, using surface air quality data, meteorological observations and ERA5 reanalysis data.

2. Data and methods

2.1. Air quality and meteorological data

We obtained surface air quality data from 2016 to 2020 for 63 cities in BTH, YRD and PRD (table S1) from the public website of the Ministry of Ecology and Environment (MEE) of China (https://air.cnemc.cn:18007/), which provides hourly O_3, $PM_{2.5}$, PM_{10}, SO_2, NO_2, and CO data. We converted O_3 concentrations after August 2018 to the original standard state (273 K and 101.325 kPa) to ensure longitudinal comparability (www.mee.gov.cn/xxgk2018/xxgk/xxgk01/201808/t20180815_629602.html).

Hourly surface meteorological data, including air temperature (T), pressure (P), wind speed (WS), wind direction (WD), relative humidity (RH) and precipitation were obtained from the meteorological monitoring network (http://data.cma.cn/). Planetary boundary layer height (PBLH), radiation, and 500 hPa geopotential height and wind data were obtained from the ERA5 (fifth generation of European Center for Medium-Range Weather Forecasts) reanalysis dataset. ERA5 is a global atmospheric reanalysis dataset with a horizontal resolution of 0.25° × 0.25° and a temporal resolution of 1 h.

To ensure a more robust analysis of O_3-temperature relationship, we implemented the following preprocessing steps on the observational data. Air quality or meteorological data that were missing for more than 6 h on a certain day were classified as missing data. When either daily O_3 or temperature data were missing, the results were excluded from the analysis of O_3-temperature correlations. All rainy days were excluded from the dataset.

2.2. Machine learning model

We employed the random forest (RF) model (Breiman 2001) to build an O_3 prediction model and further analyzed the relationships between different driving factors and O_3 concentrations. The RF model is an ensemble machine learning method based on decision trees, which mostly focuses on variable splitting or nonlinear feature combinations (Breiman 2001), and is widely used for both classification and regression tasks. The RF model employs an ensemble approach that enhances robustness and prediction accuracy, while minimizing overfitting.

In this study, we established an O_3 prediction model based on the RF model, incorporating meteorological factors, pollutant concentrations, and the latitude and longitude of urban centers as input variables. Preliminary feature screening was conducted on the input variables by removing missing values. The data were then randomly divided into training and testing sets in a 7:3 ratio. Hyperparameter optimization was performed using a grid search combined with cross-validation, ultimately constructing an O_3 concentration prediction model. The model demonstrated good predictive capability for O_3 concentrations, as illustrated in figure S1, showing strong agreement with the observed data ($r = 0.97$).

We further used feature importance and meteorological averaging methods to assess the influence of various meteorological parameters on O_3 prediction. The feature importance was quantified through the mean decrease in impurity (Gini importance). During tree construction, the algorithm tracks the total reduction in node impurity (measured by mean squared error for regression) attributable to each variable across all trees. Higher importance scores indicate stronger predictive contributions to O_3 concentration forecasts. The meteorological averaging method uses the average value of each meteorological variable to replace the original meteorological variable sample, thus forming a new average meteorological variable sample. This new sample is then used to train the optimized RF model for prediction. The difference between the predicted values obtained using the original sample (baseline) and the averaged meteorological sample (climatology) reflects the contribution of each variable to O_3 prediction performance.

2.3. Identification of ozone suppression

In general, O_3 suppression was defined as a significant reduction in the O_3-T slope at high temperature (Steiner *et al* 2010, Shen *et al* 2016, Ning *et al* 2022). In this study, we employed the Z test (Paternoster *et al* 1998) to evaluate the stationarity of O_3-T slopes for each city as follows,

$$Z = \frac{S_{\mathrm{H}} - S_{\mathrm{N}}}{\sqrt{\mathrm{SE}_{\mathrm{H}}^2 + \mathrm{SE}_{\mathrm{N}}^2}}$$

where S_{H} and S_{N} are the O_3-T slopes under high- and normal-temperature regimes, respectively, and SE_{H} and SE_{N} are the standard errors of the slopes associated with the two regimes. $|Z| > 1.96$ suggests a significant reduction in the O_3-T slope and consider it as evidence to confirm O_3 suppression in the city. We tested the threshold temperature distinguishing high- and normal-temperature using increments of 0.5 °C from the 70th to 98th percentile of the ranked T series and took the temperature with the minimum p value < 0.05 as the cut-off temperature (T_c) of the city.

In this study, we analyzed O_3 suppression on a daily scale using the maximum 8 h average (MDA8) O_3 concentration and daily maximum temperature ($T_{\max}$). We excluded data from days with precipitation or a daily maximum temperature less than 15 °C. We also detrended the observed O_3 concentration and temperature during 2016–2020 to avoid the influence of shared interannual upward trends in O_3 and temperature which would amplify their apparent positive correlation. Statistical significance in this study was evaluated using a t test with $\alpha = 0.05$.

3. Result and discussion

3.1. Observations of ozone suppression at high temperature

We analyzed the phenomenon of O_3 suppression at high temperature for 13 cities in the BTH region, 41 cities in the YRD region and nine cities in the PRD region (table S1) from 2016 to 2020.

Pronounced O_3 suppression at high temperatures was observed in the YRD and PRD regions (figure 1). Specifically, when air temperatures exceeded 30 °C and 32 °C, the O_3-T relationship exhibited a significant decline, from 4.9 μg m^{-3} °C^{-1} to −1 μg m^{-3} °C^{-1} in the YRD region and from 4.9 μg m^{-3} °C^{-1} to 2.9 μg m^{-3} °C^{-1} in the PRD region. This trend was accompanied by a decrease in O_3 concentration. The regional average O_3 concentration declined from 155 μg m^{-3} to 140 μg m^{-3} between 31 °C and 35 °C in the YRD region and from 135 μg m^{-3} to 117 μg m^{-3} between 30 °C and 33 °C in the PRD region. In contrast, the O_3-T trend was relatively stable in the BTH region; O_3 concentrations consistently increased with temperatures at a rate of ∼6 μg m^{-3} °C^{-1}, with no significant reduction at high temperatures.

Most cities mirrored the overall trends of their respective regions. Specifically, 39 of the 41 cities in the YRD region exhibited high-temperature O_3 suppression, with a cut-off temperature of 28.0 °C–34.5 °C. Notably, coastal cities experienced a lower cut-off temperature, approximately 2 °C–4 °C less than their inland counterparts. In the PRD region, high-temperature O_3 suppression was identified in 6 of the 9 cities, with cut-off temperatures of 29.0 °C–32.5 °C. Again, coastal cities such as Dongguan, Zhongshan and Zhuhai exhibited lower cut-off temperatures, approximately 2 °C lower than those of other cities. In contrast, only 4 of the 13 cities in the BTH region, Beijing, Tianjin, Baoding and Langfang, demonstrated high-temperature O_3 suppression at the city level, with notably higher cut-off temperatures of 31.0 °C–35.5 °C, approximately 4 °C higher than those observed in the PRD and YRD regions.

These results are consistent with those of previous studies (Ning *et al* 2022, Ou *et al* 2023, Fu *et al* 2024). However, minor discrepancies were observed in the results of specific cities and precise cut-off temperatures. These differences were primarily attributed to variations in the selection of representative days, such as precipitation days, and the inclusion of detrending processes.

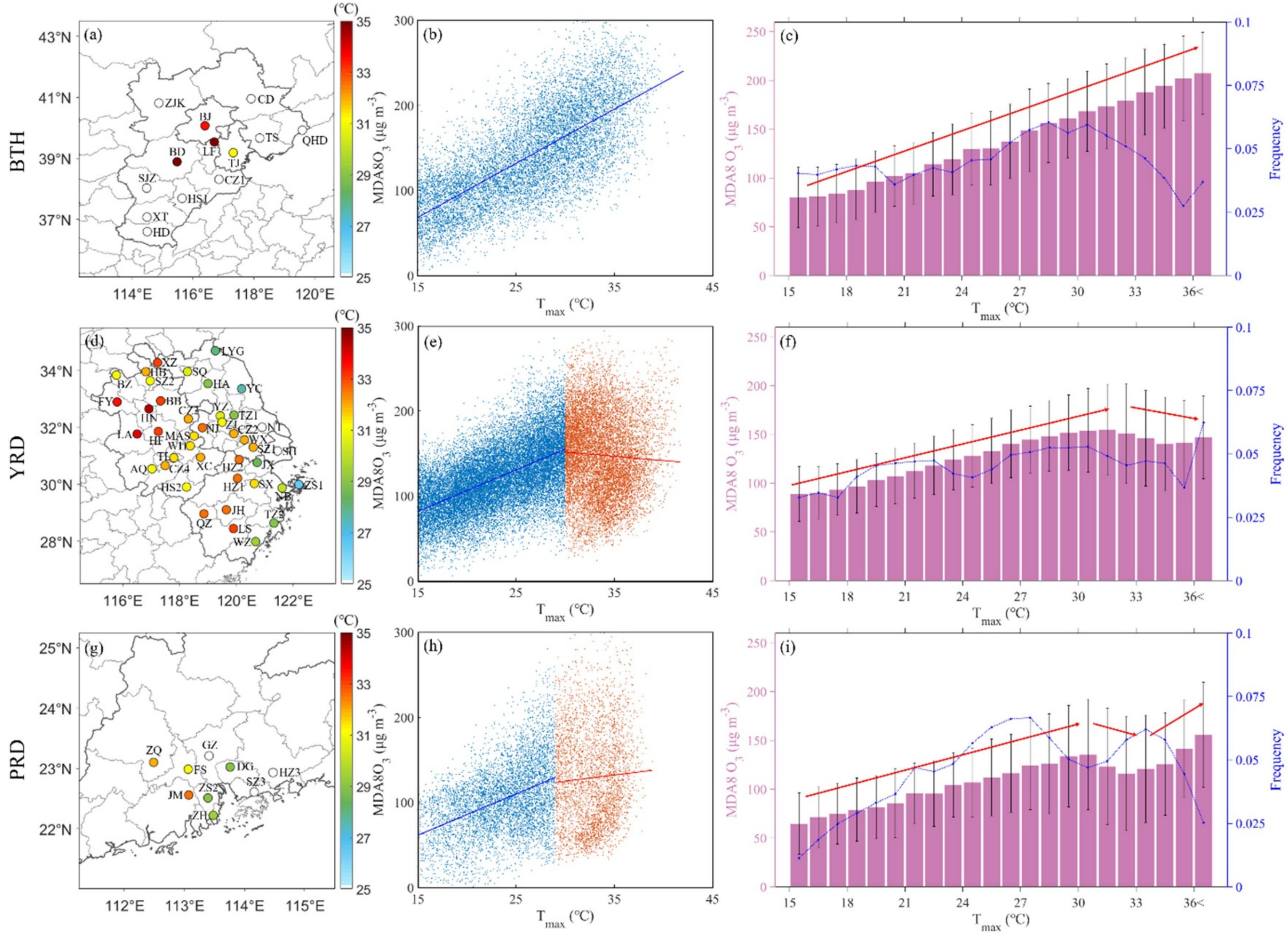

Figure 1. The observed O_3 suppression in the BTH (a)–(c), YRD (d)–(f) and PRD (g)–(i) regions of China. The left panel shows the distribution of cities across the three regions, with the colors of the dots representing the cutoff temperature at which O_3 suppression occurs at high temperatures. The middle panel shows scatter plots of T_{max} and MDA8 O_3 for each region. The right panel shows the temperature-binned MDA8 O_3 averaged for each region.

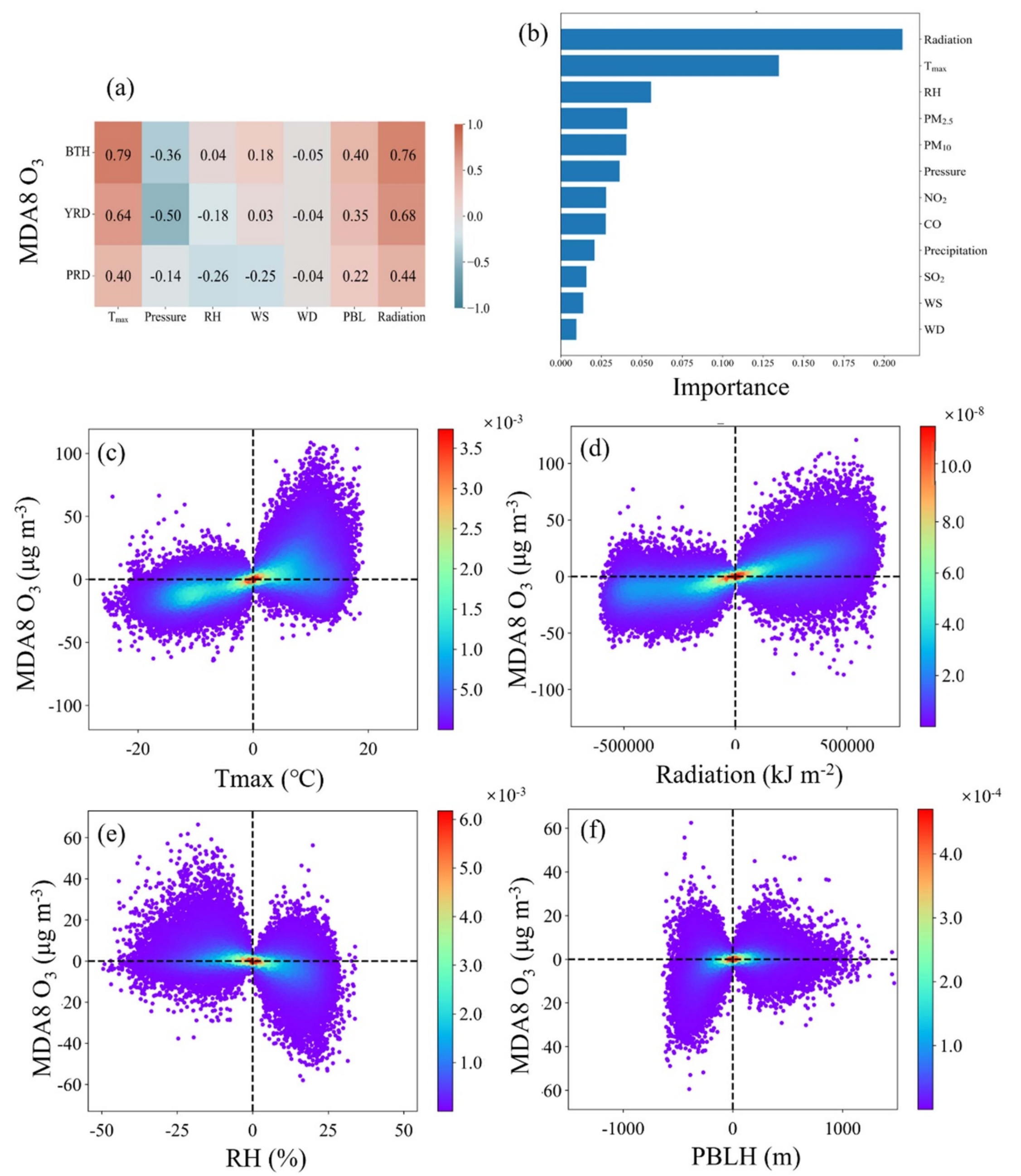

Figure 2. Relationships between MDA8 O_3 and meteorological factors. Panel a shows the correlation coefficients between MDA8 O_3 and different meteorological factors across the BTH, YRD and PRD regions, all data meet the criteria for statistical significance (p-value < 0.05). Panel (b) shows the importance of each factor in the machine learning based O_3 prediction model. Panels (c)–(f) show the O_3 responses to changes in T_{max}, radiation, RH and PBLH.

3.2. Relationships between ozone concentrations and meteorological factors

O_3 formation and transportation are intricately linked to meteorological conditions (Chen *et al* 2019). We employed three methods to analyze the relationships between O_3 and multiple meteorological factors (T, solar radiation, P, RH, WS, WD, and PBLH). (1) We calculated the correlations between meteorological factors and O_3 concentration. (2) We established a machine learning based meteorological-O_3 model, and assessing the importance of each meteorological factor in explaining changes in O_3 concentration. (3) We used the meteorological-O_3 model to perturb each meteorological factor individually and evaluate the resulting changes in O_3 concentration. By integrating these three approaches, we identified the key meteorological factors that influencing O_3 levels.

The results showed that T, radiation, P, RH, and PBLH were most closely associated with changes in O_3 concentration (approach 1, figures 2(a) and S2). O_3 demonstrated a significant positive correlation with T, radiation and PBLH, but a significant negative correlation with RH and P (p-value < 0.05). The meteorological-O_3 model corroborated these findings. The importance ranking result identified radiation, T, RH and P as the top four factors (approach 2, figure 2(b)).

Sensitivity analysis using the meteorological-O_3 model showed a significant positive feedback between O_3 concentration and perturbations in T and radiation (approach 3, figures 2(c) and (d)), particularly during O_3 polluted periods. Despite the strong collinearity between these two meteorological variables, their impacts on O_3 formation operate through distinct chemical mechanisms: radiation primarily affects photolysis rates directly, whereas temperature predominantly influences O_3 production by modulating radical reactions and balance.

We also observed a notable positive feedback between O_3 concentration and perturbations in PBLH, which contradicts the conventional understanding that a higher PBLH facilitates pollutant diffusion (Nair *et al* 2018, Su *et al* 2018, Miao *et al* 2022). The primary reason for this counterintuitive result is that, unlike other pollutants, peak O_3 formation and further concentration typically occur not at the surface, but at altitudes of approximately 0.6–1.0 km above the ground level, as suggested by unmanned aerial vehicle, O_3 LiDAR and model simulations (He *et al* 2020, Liu *et al* 2022, Guo *et al* 2024, Wang *et al* 2024). Consequently, an increased PBLH enhances the downward transport of O_3 from higher altitudes, increasing surface O_3 concentrations (Zhang and Rao 1999, Rappenglück *et al* 2008). However, the diffusion effect also plays a role; if the dilution effect exceeds the transport effect as the PBLH continues to increase, surface O_3 concentrations are ultimately reduced.

In contrast, O_3 concentration showed a significant negative feedback with perturbations in RH. Ambient humidity significantly inhibits O_3 pollution (Tong *et al* 2017, Chen *et al* 2019) through the following pathways: (1) directly scattering incoming solar radiation and indirectly increasing cloud coverage, thereby reducing the amount of O_3 reaching the surface (Noelia *et al* 2021); (2) enhancing the absorption of O_3 by plant leaves (Kavassalis and Murphy 2017, Li *et al* 2021), and (3) promoting the partitioning of NO_2- and ONO_2-containing products into the particle phase, thereby contributing to O_3 loss (Jia and Xu 2013).

The sensitivity analysis revealed no significant feedback between O_3 concentrations and perturbations in P (figure S3), despite P being identified as an important factor in both approaches 1 and 2. This lack of feedback was attributed to the inherent negative correlation between P and T, which may induce an extrinsically negative relationship between P and O_3.

3.3. Meteorological driving factors of the ozone suppression

T, radiation, RH, and PBLH were identified as the key meteorological factors influencing O_3 concentration. Therefore, we analyzed how these factors affect O_3 suppression at high temperatures and compared their impacts between regions with and without O_3 suppression.

Figure 3 illustrates the relationship between RH and O_3 in the BTH, YRD and PRD regions. In all three regions, O_3 concentrations initially remained stable then declined as RH increased (figures 3(a), (d) and (g)). According to Z test calculations (similar to those in section 2.3), O_3 concentrations exhibited a rapid decline once RH exceeded 65%–70% in the YRD and PRD regions. In contrast, O_3 concentrations in the BTH region only significantly declined once RH exceeded 80%, indicating a higher RH threshold. In addition to RH thresholds, we also observed significant regional differences in overall humidity levels and RH variations between high-temperature days (HTDs) (defined as days exceeding the cut-off temperature for cities experiencing O_3 suppression) and non-HTDs (defined as days below the cut-off temperature). In the YRD and PRD regions, the dominant RH values were 75%–80%, which surpassed the threshold for O_3 reduction, and the RH on HTDs was higher than that on non-HTDs (p-value < 0.05). This suggests a significant role of RH in O_3 suppression in these regions. Conversely, the BTH region was generally drier, with RH on most days remaining below the threshold for O_3 decline. Moreover, RH tended to be even lower on HTDs than on non-HTDs, indicating no substantial contribution to O_3 suppression.

We also examined the effects of radiation (figure S4) and PBLH (figure S5) on O_3 suppression at high temperatures across the three regions. The influence of radiation was clear and stable; O_3 concentrations increased linearly with radiation intensity, and were markedly higher on HTDs than on non-HTDs (p-value < 0.05). Thus, radiation promoted O_3 formation in all regions. The relationship between PBLH and O_3 is more complex because it is influenced by both vertical diffusion and transport effects. In general, lower PBLH values were correlated with increased O_3 concentrations due to vertical transport. However, once the PBLH exceeded a specific threshold (calculated by Z tests as: 650 m for BTH, 750 m for YRD, and 600 m for PRD), the response became more region-specific. In the BTH and PRD regions, O_3 concentrations plateaued then declined as PBLH increase, whereas O_3 levels remained stable or increased slightly as PBLH increased in the YRD region. PBLH values were higher on HTDs than on non-HTDs in all regions: $\sim$30% higher in the BTH region and 10%–15% higher in the YRD and PRD regions. As a result, PBLH changes during HTDs

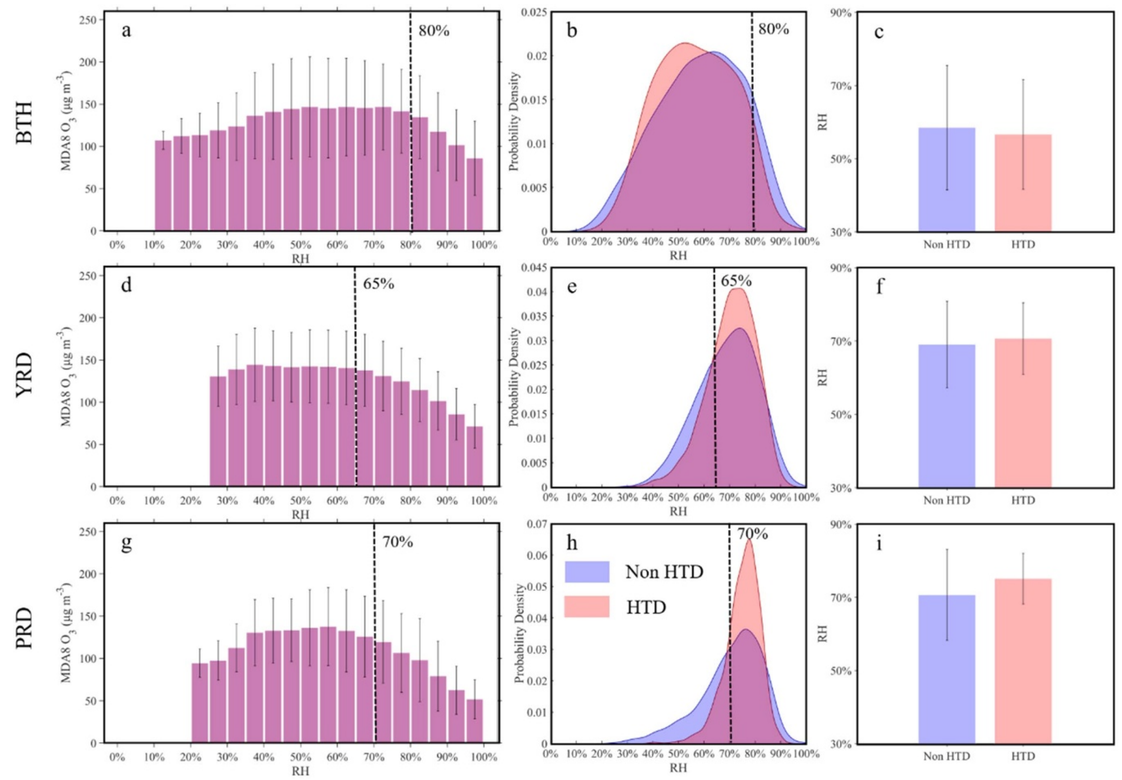

Figure 3. Changes in MDA8 O_3 concentrations at different RH levels across the BTH, YRD and PRD regions. Panels (a), (d) and (g) show the RH-binned averaged MDA8 O_3 concentrations for each region. Panels (b), (e) and (h) show the probability density of RH on high-temperature days (HTD) and non-high-temperature days (non HTD) for each region. Panels (c), (f) and (i) show the averaged RH values on HTD and non HTD for each region.

suppressed O_3 in the BTH region, but had relatively minor impacts in the YRD and PRD regions.

Based on the RH and PBLH thresholds determined through *Z* test, we categorized daily RH and PBLH values into four conditions (figure 4). Low RH combined with high PBLH represents a conducive environment for O_3, whereas high RH and low PBLH represents an inhibitory condition for O_3. Quadrant characterized by high RH and high PBLH exhibits moderate inhibition owing to the weak promotion from effect of PBLH. Quadrant with low RH and low PBLH is considered moderate. In the YRD and PRD regions, the proportion of HTDs with inhibitory and moderately inhibitory conditions was significantly higher (74%–80%) than moderate and conducive conditions (20%–26%). In contrast, the BTH region exhibited a higher proportion of HTDs in moderate and conducive conditions (95%). This discrepancy accounts for the marked O_3 suppression observed in the YRD and PRD regions, which are largely absent in the BTH region.

We also investigated the synoptic mechanisms responsible for differences in meteorological parameters between high-temperature and non-HTDs by conducting a comparative analysis of surface and 500 hPa weather conditions. On HTDs, both the YRD and PRD regions experienced a significant increase in RH (figure 5), whereas the BTH region and much of northern China show a marked decline (p-value < 0.05 for most regions, figure S6). On HTDs, southwesterly and southerly winds intensified in the YRD and PRD regions, bringing moist air from the East and South China Sea, respectively, thereby increasing local RH. In contrast, HTDs in the BTH region witnessed anticyclonic anomalies at 500 hPa, that often involved sinking airflows. Descending air is compressed, which results in increase temperature and a corresponding decrease in RH. Additionally, strong heatwaves in the PRD region are often associated with the Western Pacific Subtropical High or typhoons. These synoptic systems induce subsiding air masses, enhanced solar radiation, and weak winds, all of which contribute to the accumulation of surface O_3 (Qi *et al* 2024, figure 1(i)).

Hence, we identified RH as the dominant factor accounting for regional differences in O_3 suppression, primarily through the contrasting effects of dry heat (BTH) versus wet heat (YRD and PRD) conditions. PBLH emerged as a secondary influential factor that modulates O_3 concentration through the competitive effects of diffusion and transport processes. The meteorological factors influencing high-temperature O_3 suppression and the distinct regional disparities are visualized in figure 6.

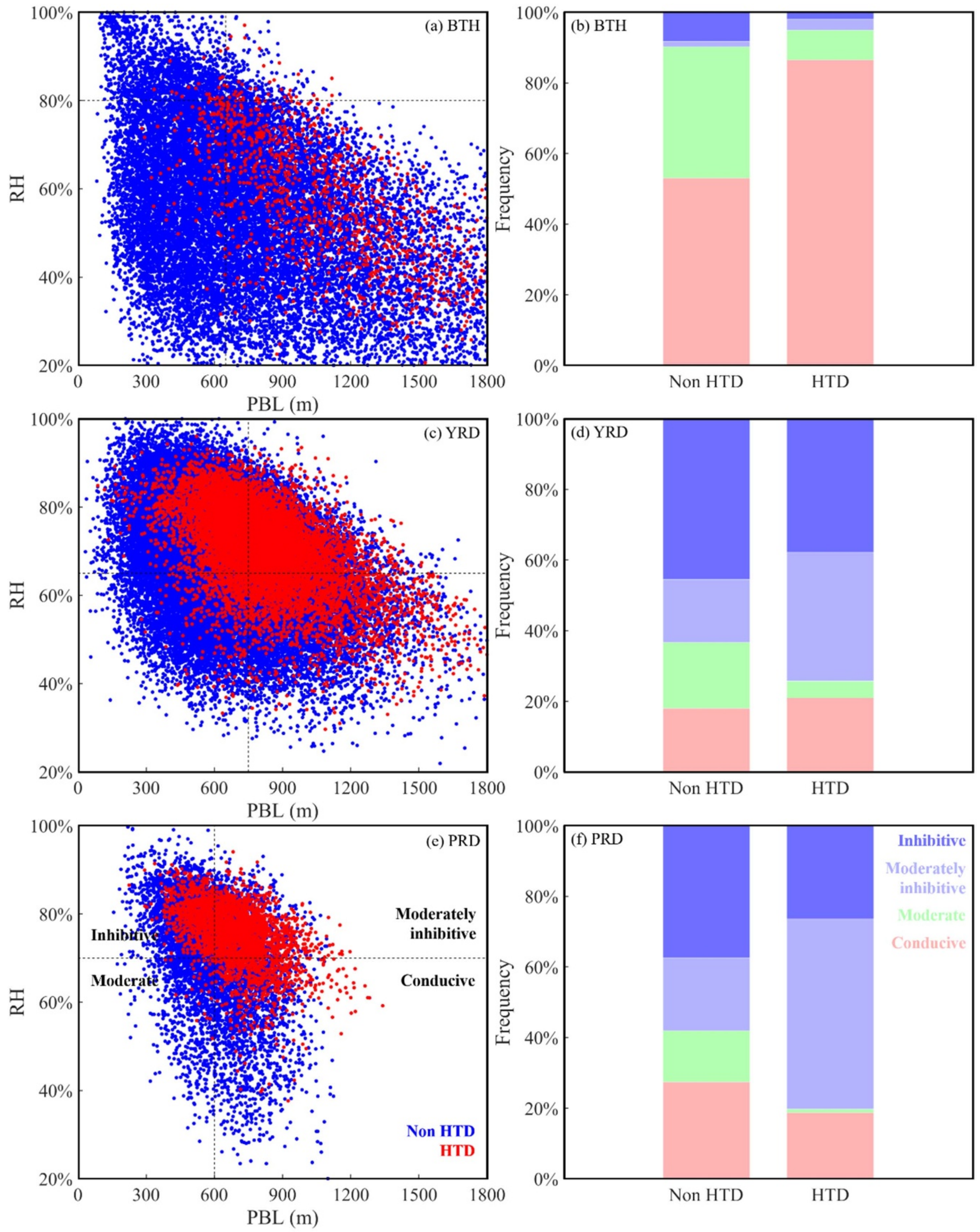

Figure 4. MDA8 O_3 distributions under different RH and PBL conditions. Panels (a), (b) and (c) show scatter plots of MDA8 O_3 versus RH and PBL for the BTH, YRD and PRD regions. Red represents high-temperature days (HTD) and blue represents non-high-temperature days (non HTD). Based on differences in RH and PBL, the data are divided into four quadrants to indicate whether conditions are conducive to O_3 pollution: inhibitive, moderately inhibitive, moderate and conducive. Panels (b), (d) and (f) compare the frequency of occurrence of these four types of days on HTD and non HTD across the three regions.

In addition to meteorological factors, chemical factors also play a crucial role in the high-temperature O_3 suppression. Notably, reduced NO_x sequestration by PAN and decreased biogenic isoprene emissions under extremely high-temperature conditions are significant contributors. However, the influence of these chemical factors exhibits high spatial variability at the city level so is difficult to accurately assess. Nevertheless, we incorporated numerical simulations to briefly compare the relative contributions of meteorological and chemical factors by simulating O_3 in the YRD region from May to June 2018 using the WRF-CMAQ model. Detailed model methods can be found in supplementary text 1. According

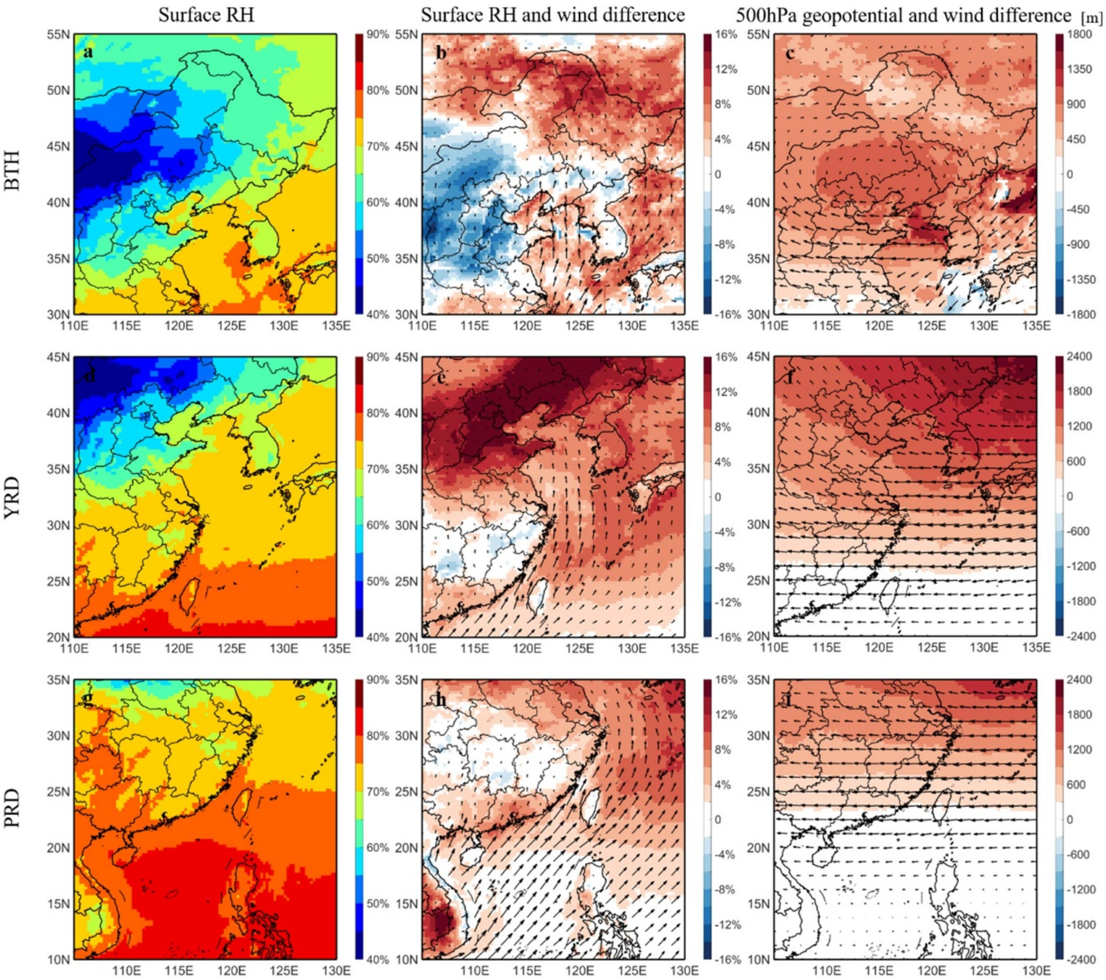

Figure 5. The spatial distributions of RH (a), (d) and (g) and the differences in RH between high-temperature days and non-high-temperature days at the surface (b), (e) and (h) and at 500 hPa (c), (g) and (i) across the BTH, YRD and PRD regions. The overlaid arrows represent the differences in wind patterns.

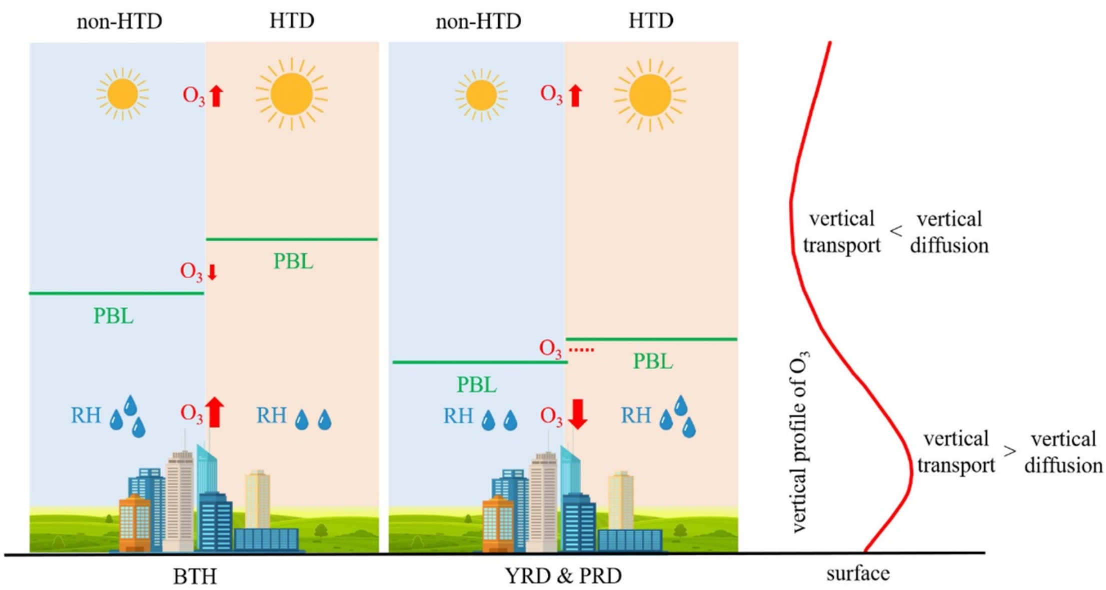

Figure 6. A conceptual scheme for meteorological mechanism of high temperature O_3 suppression in different regions. HTD represents high-temperature days.

to a process analysis of O_3 generation (figure S7), the contribution of horizontal and vertical transport processes (meteorologically driven) to the O_3 formation rate decreased by 1.91 μg m^{-3} hr^{-1} during HTDs, whereas that of chemical processes (jointly influenced by chemistry and meteorology, e.g. radiation) increased by 1.41 μg m^{-3} hr^{-1}. Thus, we can infer that meteorological factors demonstrated greater influence on high-temperature O_3 suppression than chemical factors, although precisely quantifying their independent contributions remains challenging.

4. Conclusion and discussions

O_3 concentrations generally increase with increasing temperature and radiation. However, many observational evidences suggest that under extreme high-temperature conditions, O_3 pollution does not continue to rise with temperature but instead tends to plateau or even decline. Understanding the mechanisms underlying O_3 suppression at high temperatures is crucial for effective O_3 pollution control, particularly in the context of ongoing climate warming and increasingly frequent heatwaves.

In this study, we used surface air quality data, meteorological observations, and ERA5 reanalysis data from typical regions of Eastern China (BTH, YRD and PRD) for the period 2016–2020 to explore the attributes of O_3 suppression under high-temperature conditions and the meteorological factors driving this phenomenon in different regions. The results indicated significant high temperature O_3 suppressions in the YRD and PRD regions, with a cut-off temperature of 28.0 °C–34.5 °C. In contrast, high-temperature O_3 suppression was rarely observed in the BTH region, affecting only 4 of the 13 cities, and the cut-off temperature was ~4 °C higher than that in the YRD and PRD regions. According to statistical analysis and machine learning model, the key meteorological factors associated with changes in O_3 concentrations in Eastern China were *T*, radiation, RH, and PBLH. Among these, RH was the primary driver of regional differences in O_3 suppression, followed by PBLH. In the YRD and PRD regions, the influence of warm and humid air from the south increased the RH on HTDs relative to non-HTDs, which further contributed to notable high-temperature O_3 suppression in both regions. In contrast, HTDs in the BTH region were often associated with the presence of upper-level anticyclones, which resulted in dry, descending airflows that reduced the RH, thereby increasing O_3 concentrations. Furthermore, joint cluster analysis of RH and PBLH revealed that inhibitory conditions were more common on HTDs (74%–80%) than on non-HTDs (58%–63%) in YRD and PRD regions, whereas conditions that favorable for O_3 accumulation were more common on HTDs (86%) than on non-HTDs (53%) in the BTH region.

Data availability statement

All data that support the findings of this study are included within the article (and any supplementary files).

Acknowledgment

This work was supported by the National Key R&D Program of China (2022YFC3701005), the Natural Science Foundation of Jiangsu Province (Grant No. BK20220031) and the special fund of Key Laboratory of Formation and Prevention of Urban Air Pollution Complex, MEE (SEPAir-2024080216).

Conflict of interest

Conflict of interest the authors declare no competing interests.

Open research

The air quality data used in this study are publicly available at the public website of the MEE of China (https://air.cnemc.cn:18007/). The meteorological data used in this study are publicly available at the public website of ECMWF (www.ecmwf.int/en/forecasts/dataset/ecmwf-reanalysis-v5).

ORCID iDs

Nan Li 0000-0003-3052-4414
Jiandong Li 0000-0002-5857-8177
Hong Liao 0000-0001-6628-1798

References

Atkinson R W *et al* 2016 Long-term exposure to ambient ozone and mortality: a quantitative systematic review and meta-analysis of evidence from cohort studies *BMJ Open.* **6** e009493

Breiman L 2001 Random forests *Mach. Learn.* **45** 5–32

Chen Z, Zhuang Y, Xie X, Chen D, Cheng N, Yang L and Li R 2019 Understanding long-term variations of meteorological influences on ground ozone concentrations in Beijing during 2006–2016 *Environ. Pollut.* **245** 29–37

Feng Z *et al* 2022 Ozone pollution threatens the production of major staple crops in East Asia *Nat. Food* **3** 47–56

Feng Z, Marco D A, Anav A, Gualtieri M, Sicard P, Tian H, Fornasier F, Tao F, Guo A and Paoletti E 2019 Economic losses due to ozone impacts on human health, forest productivity and crop yield across China *Environ. Int.* **131** 104966

Fu W *et al* 2024 Recent-year variations in O_3 pollution with high-temperature suppression over central China *Environ. Pollut.* **349** 123932

Gu Y, Li K, Xu J, Liao H and Zhou G 2020 Observed dependence of surface ozone on increasing temperature in Shanghai, China *Atmos. Environ.* **221** 117108

Guo W, Zhu L Y, Li Y Y, Chen L, Yan S M and Li Y G 2024 Vertical distribution characteristics of O_3 under diverse polluted weather based on unmanned aerial vehicle observations *China Environ. Sci.* **44** 6578–89

Han H, Liu J, Shu L, Wang T and Yuan H 2020 Local and synoptic meteorological influences on daily variability in summertime surface ozone in Eastern China *Atmos. Chem. Phys.* **20** 203–22
He G W *et al* 2020 Characterizing the near-surface vertical variations of summertime O_3 in Jiaxing *China Environ. Sci.* **40** 4265–74
Hu C, Kang P, Jaffe D A, Li C, Zhang X, Wu K and Zhou M 2021 Understanding the impact of meteorology on ozone in 334 cities of China *Atmos. Environ.* **248** 118221
Jia L and Xu Y 2013 Effects of relative humidity on ozone and secondary organic aerosol formation from the photo oxidation of benzene and ethylbenzene *Aerosol Sci. Technol.* **48** 1–12
Kavassalis S C and Murphy J G 2017 Understanding ozone-meteorology correlations: a role for dry deposition *Geophys. Res. Lett.* **44** 2922–31
Li K, Jacob D J, Liao H, Shen L, Zhang Q and Bates K H 2019 Anthropogenic drivers of 2013–2017 trends in summer surface ozone in China *Proc. Natl Acad. Sci.* **116** 422–7
Li M *et al* 2021 Large scale control of surface ozone by relative humidity observed during warm seasons in China *Environ. Chem. Lett.* **19** 3981–9
Liu H L, Han X, Tang G Q, Zhang J Q, Xia X A, Zhang M G and Meng L H 2022 Model analysis of vertical exchange of boundary layer ozone and its impact on surface air quality over the North China Plain *Sci. Total Environ.* **821** 153436
Liu P, Song H, Wang T, Wang F, Li X, Miao C and Zhao H 2020 Effects of meteorological conditions and anthropogenic precursors on ground-level ozone concentrations in Chinese cities *Environ. Pollut.* **262** 114366
Lu X, Hong J, Zhang L, Cooper O R, Schultz M G, Xu X, Wang T, Gao M, Zhao Y and Zhang Y 2018 Severe surface ozone pollution in China: a global perspective *Environ. Sci. Technol. Lett.* **5** 487–94
Meehl G A, Tebaldi C, Tilmes S, Lamarque J F, Bates S, Pendergrass A and Lombardozzi D 2018 Future heat- waves and surface ozone *Environ. Res. Lett.* **13** 064004
Miao Y, Che H, Liu S and Zhang X 2022 Heat stress in Beijing and its relationship with boundary layer structure and air pollution *Atmos. Environ.* **282** 119159
Mousavinezhad S, Choi Y, Pouyaei A, Ghahremanloo M and Nelson D L 2021 A comprehensive investigation of surface ozone pollution in China, 2015–2019: separating the contributions from meteorology and precursor emissions *Atmos. Res.* **257** 105599
Murray C J *et al* 2020 Global burden of 87 risk factors in 204 countries and territories, 1990–2019: a systematic analysis for the global burden of disease study 2019 *Lancet* **396** 1223–49
Nair S K, Madhusoodanan M S and Mehajan R K 2018 The role of boundary layer height (BLH) variations on pollution dispersion over a coastal station in the Southwest Peninsular India *J. Atmos. Sol.-Terr. Phys.* **179** 273–80
Ning G, Wardle D A and Yim S H L 2022 Suppression of ozone formation at high temperature in China: from historical observations to future projections *Geophys. Res. Lett.* **49** e2021GL097090
Noelia O, Henning W R and Tim B 2021 Temperature dependence of tropospheric ozone under NO_x reductions over Germany *Atmos. Environ.* **253** 118334
Ou L, Chen W, Wu Y, Wu L and Wang X 2023 Spatio-temporal characteristics and influencing factors of ozone suppression events under high temperature in China *Huan Jing Ke Xue* **44** 6586–97
Paternoster R, Brame R, Mazerolle P and Plquero A 1998 Using the correct statistical test for the equality of regression coefficients *Criminology* **36** 859–66
Pu X, Wang T J, Huang X, Melas D, Zanis P, Papanastasiou D K and Poupkou A 2017 Enhanced surface ozone during the heat wave of 2013 in Yangtze River Delta region, China *Sci. Total Environ.* **603–604** 807–16
Qi C N, Wang P Y, Yang Y, Li H M, Zhang H, Ren L L, Jin X P, Zhan C C, Tang J P and Liao H 2024 Impacts of tropical cyclone–heat wave compound events on surface ozone in Eastern China: comparison between the Yangtze River and pearl River deltas *Atmos. Chem. Phys.* **24** 11775–89
Rappenglück B, Perna R, Zhong S and Morris G A 2008 An analysis of the vertical structure of the atmosphere and the upper-level meteorology and their impact on surface ozone levels in Houston, Texas *J. Geophys. Res.* **113** D17315
Romer P S *et al* 2018 Effects of temperature-dependent NO_x emissions on continental ozone production *Atmos. Chem. Phys.* **18** 2601–14
Shen L, Mickley L J and Gilleland E 2016 Impact of increasing heat waves on U.S. ozone episodes in the 2050s: results from a multimodel analysis using extreme value theory *Geophys. Res. Lett.* **43** 4017–25
Steiner A L, Davis A J, Sillman S, Owen R C, Michalak A M and Fiore A M 2010 Observed suppression of ozone formation at extremely high temperatures due to chemical and biophysical feedbacks *Proc. Natl Acad. Sci.* **107** 19685–90
Su T, Li Z and Kahn R 2018 Relationships between the planetary boundary layer height and surface pollutants derived from lidar observations over China: regional pattern and influencing factors *Atmos. Chem. Phys.* **18** 15921–35
Sun H Z, Yu P, Lan C, Wan M W L, Hickman S, Murulitharan J, Shen H, Yuan L, Guo Y and Archibald A T 2022 Cohort-based long-term ozone exposure-associated mortality risks with adjusted metrics: a systematic review and meta-analysis *Innovation* **3** 100246
Tai A P K, Martin M V and Heald C L 2014 Threat to future global food security from climate change and ozone air pollution *Nat. Clim. Change* **4** 817–21
Tong L, Zhang H, Yu J, He M, Xu N, Zhang J, Qian F, Feng J and Xiao H 2017 Characteristics of surface ozone and nitrogen oxides at urban, suburban and rural sites in Ningbo, China *Atmos. Res.* **187** 57–68
Wang Q, Jing K, Wang C J, Liu B X, Shen X E, Zhang J, Liu Y and Luo X X 2024 Vertical distribution of ozone in lower atmosphere in summer in the Southeastern suburb of Beijing *Res. Environ. Sci.* **37** 686–95
Wang T, Xue L, Brimblecombe P, Lam Y F, Li L and Zhang L 2017 Ozone pollution in China: a review of concentrations, meteorological influences, chemical precursors, and effects *Sci. Total Environ.* **575** 1582–96
Wang T, Xue L, Feng Z, Dai J, Zhang Y and Tan Y 2022 Ground-level ozone pollution in China: a synthesis of recent findings on influencing factors and impacts *Environ. Res. Lett.* **17** 063003
Wang Y, Wang Y, Feng Z, Yuan X and Zhao Y 2023 The impacts of ambient ozone pollution on China's wheat yield and forest production from 2010 to 2021 *Environ. Pollut.* **330** 121726
Xu J, Huang X, Wang N, Li Y and Ding A 2021 Understanding ozone pollution in the Yangtze River Delta of Eastern China from the perspective of diurnal cycles *Sci. Total Environ.* **752** 141928
Zhang J and Rao S T 1999 The role of vertical mixing in the temporal evolution of ground-level ozone concentrations *J. Appl. Meteorol.* **38** 1674–91